

Paper:

# Quadrotor Drone Hovering in Ground Effect

Yasutada Tanabe<sup>\*1</sup>, Hideaki Sugawara<sup>\*1</sup>, Shigeru Sunada<sup>\*2</sup>,  
Koichi Yonezawa<sup>\*3</sup>, and Hiroshi Tokutake<sup>\*4</sup>

<sup>\*1</sup>Japan Aerospace Exploration Agency (JAXA)

6-13-1 Osawa, Mitaka, Tokyo 181-0015, Japan

E-mail: tan@chofu.jaxa.jp

<sup>\*2</sup>Nagoya University

Furo-cho, Chikusa-ku, Nagoya, Aichi 464-8603, Japan

<sup>\*3</sup>Central Research Institute of Electric Power Industry (CRIEPI)

1646 Abiko, Abiko-shi, Chiba 270-1194, Japan

<sup>\*4</sup>Kanazawa University

Kakuma-machi, Kanazawa, Ishikawa 920-1192, Japan

[Received October 10, 2020; accepted January 19, 2021]

**A variable-pitch-controlled quadrotor drone was simulated in the ground effect using a high-fidelity CFD solver. In contrast to a single rotor in the ground effect, which has been extensively studied for conventional helicopters, the flow fields around multiple rotors are complex. In this study, the rotating speed of the rotors was maintained constant, and the blade pitch angles were adjusted so that the total thrust of the multicopter was the same regardless of the rotor height from the ground. It was observed that the power required for the quadrotors, which generate the same thrust, decreases when the rotors are approaching the ground from the height where they can be considered to be out of the ground effect, but increases locally when the rotor height is approximately the rotor radius, owing to flow recirculation into the rotor, and then decreases abruptly when the rotors further approach the ground. The outwash from the quadrotors depends heavily on the direction relative to the quadrotor layout. Along the plane crossing the diagonal rotor centers, the outwash velocity profiles resemble those of a single rotor; however, the outwash from the rotor gaps is stronger and extends to a much higher altitude.**

**Keywords:** quadrotor drone, CFD simulation, ground effect, variable pitch control

## 1. Introduction

Multicopter-type drones have been employed in various fields. Larger drones weighing more than 30 kg have been developed mainly for transportation and agricultural spraying. Meanwhile, electric vertical take-off and landing (eVTOL) aircraft aiming for personnel transportation are being studied and are under development worldwide. Uber proposed using eVTOL as an air taxi to carry up to

five persons [a]. The weights of the aircraft proposed by several Uber Elevate partners were over 2000 kg [b].

As the weight of the rotorcraft increases, safety concerns associated with downwash arise. The downwashes caused by conventional helicopters are dominated by single main rotors, which have been extensively studied. The velocities induced in the rotors are mostly limited to less than 15 m/s to avoid accidents caused by rotor outwash on the ground during operations. The maximum outwash speed on the ground is twice the induced velocity [1]. It is likely that a wind speed of 30 m/s is considered an acceptable limit in the conventional helicopter design. When the rotor approaches the ground, the influence of the ground begins to appear. For a single rotor generating a constant thrust, the required rotor power decreases when the rotor height is less than one diameter of the rotor. Numerous studies on the helicopter ground effect and the associated downwash have been conducted so far [1–7]. A generalized model of downwash induced by a single rotor was proposed by Tanabe et al. [1]. Good correlations with the experimental tests and CFD simulations were observed.

The flow field around a multicopter tends to be extremely complex. Neighboring rotors turn in a different direction from each other. Interactions between the rotors exist [8]. When the rotor is in the ground effect, the interaction between the rotor and ground becomes dominant. As reported by Kohno et al. [9], where the quadrotors in the ground effect were studied, the distance between the rotors significantly influenced the trend of the ground effect. When the rotor gap is minimal, the overall thrust increases monotonically as the rotor height decreases, similar to the ground effect of a single rotor. When the rotor gap is greater than 0.3 times the rotor radius, the overall thrust gradually decreases as the rotor height decreases. At a rotor height less than the rotor radius, the overall thrust increases abruptly. This trend deviates significantly from that of a single rotor. It is observed that there is flow recirculation as a result of the interaction between the rotor and the ground plane, which causes the loss of the ro-





Fig. 1. Pitch-controlled quadrotor drone [11].



Fig. 2. Rotor blade shape.

tor thrust at the intermediate rotor height [10]. This trend is considered one of the causes of the flight instability of the multicopter near the ground. However, the fuselage at the center of the quadrotors was not considered, the rotors were fixed-pitch propellers, and the rotating speed was constant in previous studies. When the rotor height changes, the rotor thrust changes such that the balance between the aircraft gravitational force and the rotor thrust cannot be satisfied. More realistic simulations in which a constant thrust is generated by trimming the rotor pitch angle for a variable-pitch-controlled drone are conducted in this study.

The objectives of this study are 1) to validate the numerical methods by comparing the results of simulations of a single rotor with existing experimental measurements; 2) to obtain detailed flow field observations of the quadrotor drone hovering in the ground effect; 3) to determine the change in the required power of a quadrotor drone with the rotor height; and 4) to obtain the velocity profile on the ground due to the outwash from the quadrotor drone.

## 2. Quadrotor Drone Modeling

A photograph of a drone with four pitch-controlled rotors is shown in Fig. 1 [11]. The pitch control of the rotors was adopted to attain a fast attitude change of the drone so that it will be more robust during flight in gusty wind. In addition, the stability of the drone can be maintained during descent flight before landing. A cambered thin airfoil (OA117) was chosen, and the rotor blade had a linear twist of  $-21^\circ$ , as shown in Fig. 2.

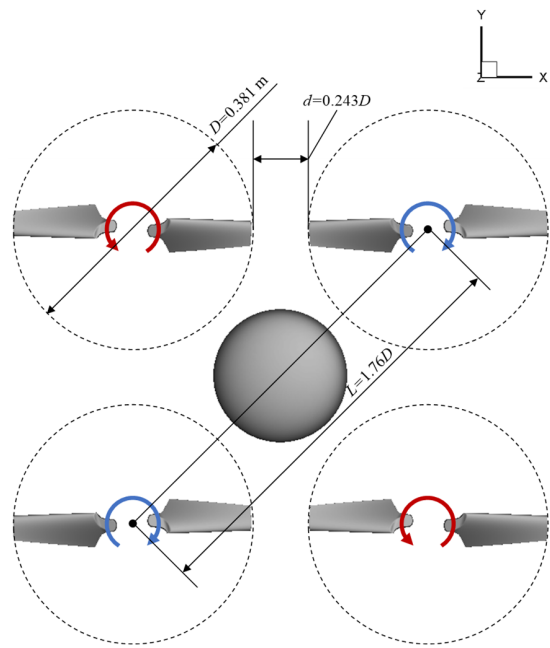


Fig. 3. Layout of the quadrotor drone.

Table 1. Drone design parameters.

Number of rotors $N_R$	4
Rotor radius $R$	0.1905 m
Blade root chord $c_r$	0.0665 m
Blade tip chord $c_t$	0.0402 m
Rotor rotational speed	5400 rpm
Number of blades $N_b$	2
Blade airfoil	OAF117
Blade twist $\theta_t$	$-21^\circ$ (linear)

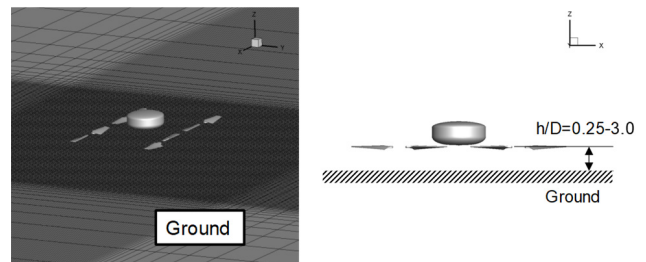


Fig. 4. Computational model of a quadrotor drone.

The layout of the quadrotor drone is illustrated in Fig. 3. The rotor diameter  $D$  is 0.381 m. The distance between diagonal rotor centers  $L$  is  $1.76D$ . The rotor gap  $d$  is  $0.243D$ . The design parameters of the drone are listed in Table 1. The rotor rotating speed is 5400 rpm. The design gross weight of this drone is 7 kg so that each rotor generates an average thrust of 17.15 N during hovering flight.

A simplified computational model based on the drone is shown in Fig. 4. The support arms, landing skids, and

**Table 2.** Computational conditions.

Rotor thrust $T$	17.15 N ( $C_T = 0.0106$ )
Control	Collective pitch $\theta_0$
Distance of rotor to ground	$h/D = 0.25, 0.50, 0.75, 1.0, 2.0, 3.0,$ OGE

other details were omitted. Only the rotor blades and central fuselage were considered. The rotor height from the ground was varied from  $0.25D$  to  $3D$ , as listed in **Table 2**. As a reference, the case without a ground plane (out-of-ground effect, referred to as OGE) was also simulated.

### 3. Numerical Methodologies

Numerical simulations of the quadrotor drone in the ground effect were conducted using a CFD code, rFlow3D, developed at JAXA specifically for rotorcraft [12]. In the rFlow3D code, a three-dimensional moving overlapping grid method is used. The blade grids move and deform within the inner Cartesian background grid. A wide outer-background Cartesian grid is used to preserve the uniform inflow condition. A static fuselage grid is placed inside the inner background. For complex fuselage shapes, a fuselage grid can be formed using an unstructured grid. In this case, the FaSTAR [13] or TAS-code [14] solver was used for the unstructured grid. A numerical solution was obtained via an interpolation from the inner grids to the outer grid. The update of the flow solution is obtained based on the boundary conditions interpolated from the outer grid. Any number of rotors can be handled using this code. rFlow3D successfully captured the interactions of a hex-rotor drone hovering near a side wall or an upper wall [15]. Further details of the computational methods applied to multiple rotors can be found in [15].

An all-speed numerical scheme, namely, simple low-dissipation AUSM (SLAU) [16] with extension to three-dimensional moving grids (referred to as mSLAU), is adopted [17]. It is suitable for flow calculation around a rotary wing, where the local flow speed may vary from very low on the root area to transonic at the tip. Combining SLAU with a fourth-order compact MUSCL TVD (FCMT) interpolation scheme [18], fourth-order spatial accuracy was obtained in shock-free regions. The implicit LU-SGS and dual-time-stepping methods [19] are used for time integration on blade grids. However, for the background grids, an explicit four-stage Runge-Kutta time integration method [20] was used. In this study, no turbulence model was adopted considering the relatively low Reynolds numbers on the rotors. The numerical methodologies applied to each type of grid are summarized in **Table 3**.

The forces and moments generated by a single rotor are nondimensionalized, as expressed in Eqs. (1)–(4), where  $C_T$  is the thrust coefficient,  $C_Q$  is the torque coefficient,

**Table 3.** Numerical methodologies.

Items	Cartesian background grid	Body-fitted grid (blade/fuselage)
Governing equations	Three-dimensional compressible Navier-Stokes equations	
Spatial discretization	Cell-vertex FVM	Cell-centered FVM
Time integration	Four-stage Runge-Kutta method	Dual-time stepping / LU-SGS
Numerical flux	mSLAU (modified SLAU)	
Reconstruction	FCMT (fourth-order compact MUSCL TVD)	
Viscous flux	Second-order central difference method	
Turbulence model	Not applied (QDNS, Quasi-DNS)	

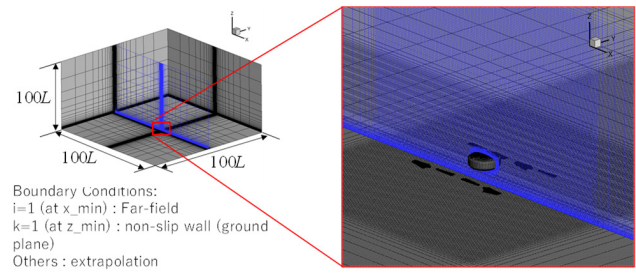


**Fig. 5.** Computational grids and boundary conditions for a quadrotor drone in the ground effect.

and  $C_P$  is the power coefficient. The figure of merit ( $FM$ ) of a rotor is defined as the ratio of the ideal induced power to the actual required power; the closer it is to 1, the better is the rotor performance in hover.

$$C_T = \frac{T}{(\rho \pi R^2 V_{tip}^2)} \dots \dots \dots (1)$$

$$C_Q = \frac{Q}{(\rho \pi R^2 V_{tip}^2 R)} \dots \dots \dots (2)$$

$$C_P = \frac{P}{(\rho \pi R^2 V_{tip}^3)} = C_Q \dots \dots \dots (3)$$

$$FM \text{ (Figure of Merit)} = \frac{\left(\frac{C_T}{\sqrt{2}}\right)^{\frac{3}{2}}}{C_P} \dots \dots \dots (4)$$

The computational grid system used in this study is shown in **Fig. 5**. The boundary conditions applied to the background surfaces are indicated. The grid geometries for the blades (8 in total) and fuselage are shown in **Fig. 6**. The resolution in the background grid around the rotors was set to 15% of the length of the blade tip chord. Dense

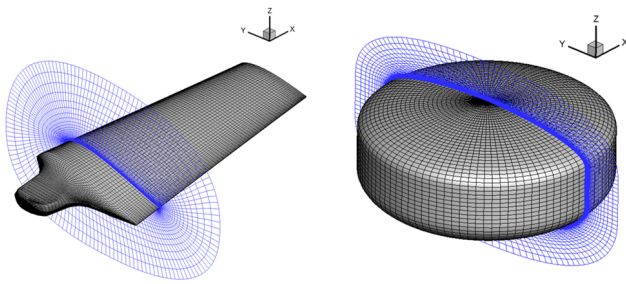


**Fig. 6.** Grid geometries for the blade (left) and the fuselage (right).

**Table 4.** Grid points and 1st cell height.

Grid	Number of grid points ( $X \times Y \times Z$ )	Height of 1st cell from the wall [m]
Background grid	$449 \times 449 \times 333$	$1.0 \times 10^{-3}$
Blade grid $\times 8$	$121 \times 143 \times 61$ (Span $\times$ Chord $\times$ Normal)	$2.0 \times 10^{-6}$
Fuselage grid	$71 \times 101 \times 45$ (Longitudinal $\times$ Circumference $\times$ Normal)	$2.0 \times 10^{-5}$

grids were placed near the walls to resolve the boundary layer flows on the blade and fuselage surface and on the ground, as presented in **Table 4**.

#### 4. Single Rotor in Ground Effect

A single rotor in the ground effect has been studied by various researchers [1–7]. The outwash on the ground was measured and modeled. The results are consistent with each other, suggesting that the ground effect and outwash profile are not sensitive to the rotor blade design [1]. However, the aspect ratio of the current blade was approximately 3. This is significantly lower than that of a conventional rotor blade, for which an aspect ratio of more than 10 is common. It is meaningful to confirm whether the conventional ground-effect empirical relations also hold for this rotor. The flow field around a single rotor provides a baseline to investigate the flow fields around multiple rotors further.

The rotor performance, namely the  $C_T$  vs.  $C_Q$  curve, of this rotor OGE was compared with the measurement, as shown in **Fig. 7**, where a blade with a twist angle of  $-21^\circ$  was adopted in the present study, and good agreement was obtained [21].

The flow fields around a single rotor near the ground are shown in **Fig. 8**. The rotor blade tip vortices are visualized with iso-Q criterion surfaces and colored by the downward velocity  $w$ , which is normalized by the sonic speed. There was no rotor-wake recirculation. The downwash induced by the rotor spreads along the ground plane

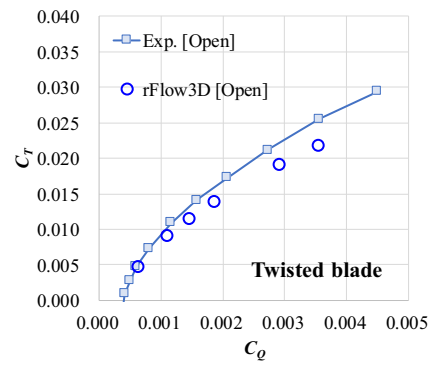


**Fig. 7.** Comparison of rotor performance between CFD prediction and measurement [21].

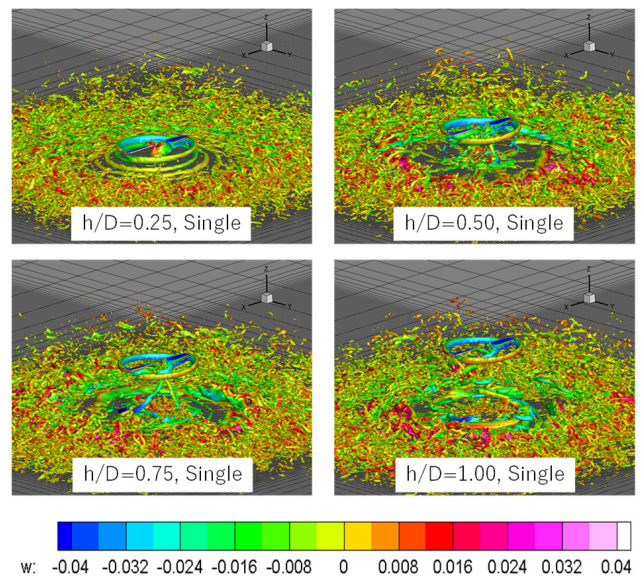


**Fig. 8.** Flow field around a single rotor near the ground.

for all rotor heights.

The required power for a single rotor generating the same thrust for various rotor heights is shown in **Fig. 9**. The prediction matches very well with the empirical relationship proposed by Schmaus et al. [6], who studied the ground effect of a rotor for man-powered rotorcraft up to distances close to the ground. The power change with respect to the rotor height is given by Eqs. (5) and (6):  $C_{p0}$  is the power coefficient when no rotor thrust is generated.

$$C_p = k_g k_{\lambda_i} C_T + C_{p0} \dots \dots \dots (5)$$

$$\left( \frac{P_{IGE} - P_0}{P_{OGE} - P_0} \right) = 0.146 + 2.090 \left( \frac{h}{R} \right) - 2.068 \left( \frac{h}{R} \right)^2 + 0.932 \left( \frac{h}{R} \right)^3 - 0.157 \left( \frac{h}{R} \right)^4 \dots \dots \dots (6)$$

The vertical velocity component on the rotor central section at 30 rotor revolutions from the start is shown in **Fig. 10**. The vertical velocity  $w$  is normalized by the sonic speed. It can be observed that the wake on the ground was unsteady. The flow speed averaged from 37 to 42

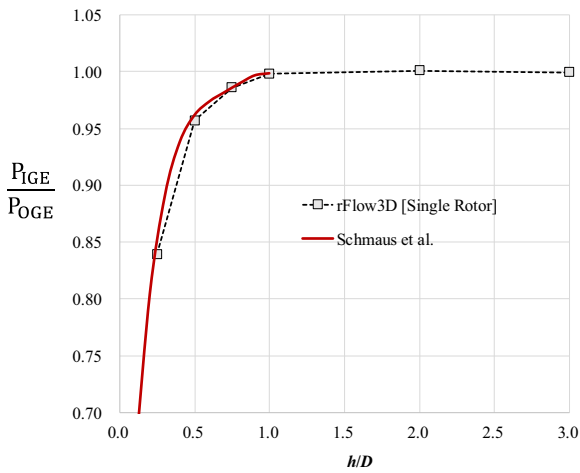


Fig. 9. Power change with ground height for a single rotor.

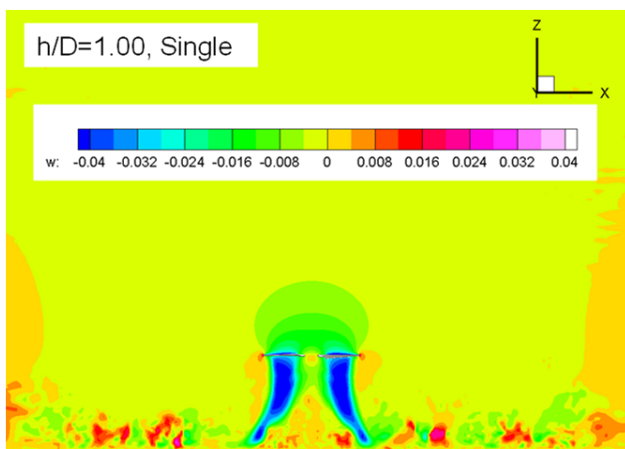


Fig. 10. Velocity distribution in the central section of a single rotor.

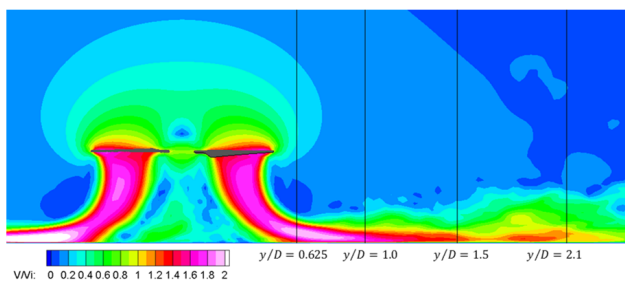


Fig. 11. Averaged flow in the central section.

revolutions normalized by the rotor-induced speed ( $v_i = \sqrt{T/2\rho A}$ ,  $\rho$ : air density;  $A$ : rotor disc area) is shown in Fig. 11. The velocity fluctuations are almost eliminated. The averaged velocity profiles at stations  $y/D = 0.625$ , 1.0, 1.5, and 2.1 are shown in Fig. 12. Compared with the measurements with a model rotor at NDA [5] and those with a real helicopter conducted by NASA [3], good agreements are obtained, except for  $y/D = 2.1$ , where the rotor downwash is considered not sufficiently developed in the numerical simulations. Please be noted that the

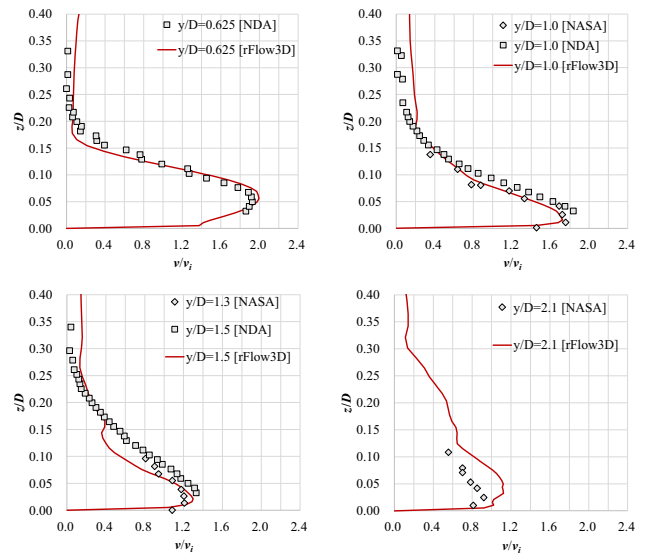


Fig. 12. Outwash profile comparisons for a single rotor.

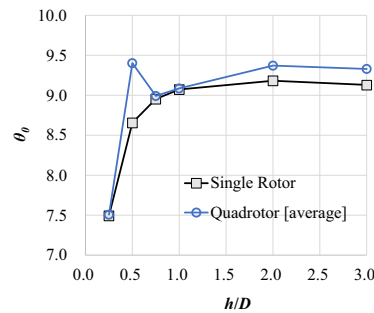


Fig. 13. Rotor pitch angle vs. rotor height.

NASA field measurement was carried out at  $y/D = 1.3$  and the NDA laboratory measurement was at  $y/D = 1.5$ . These velocity profiles are compared with the present prediction at  $y/D = 1.5$ .

### 5. Quadrotor Drone in Ground Effect

The simulations of the quadrotor drone in the ground effect are conducted in such a way that each rotor is trimmed to generate the same thrust as that of a single rotor. The rotor rotating speed was assumed to be constant; consequently, the rotor blade pitch angles were adjusted. As shown in Fig. 13, compared with the single-rotor case where a monotonic decrease in the required pitch angle with a decrease in rotor height is observed, the required average pitch angle of the quadrotor has a peak at  $h/D = 0.5$ . The rotor blade pitch angle is strongly associated with the required rotor power. The reason for the locally peaky rotor power requirement will be discussed below along with a detailed observation of the flow fields around the multiple rotors.

The instantaneous flow fields around the quadrotor drone at various rotor heights from the ground are shown

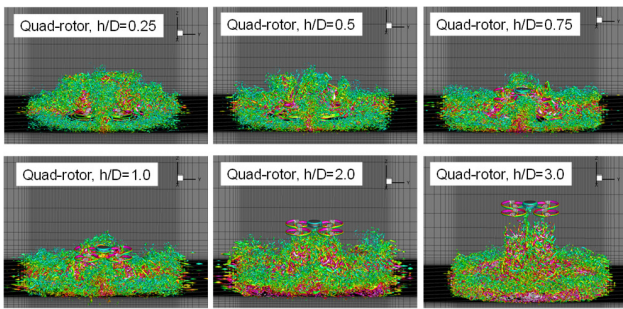


**Fig. 14.** Flow fields around a quadrotor drone at various rotor heights from the ground.

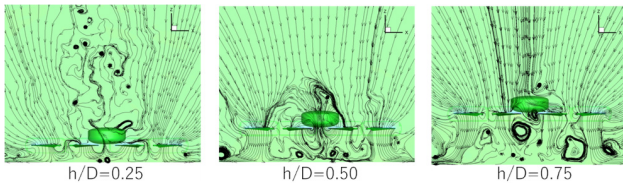


**Fig. 15.** Streamlines projected onto the plane crossing two neighboring rotor centers.

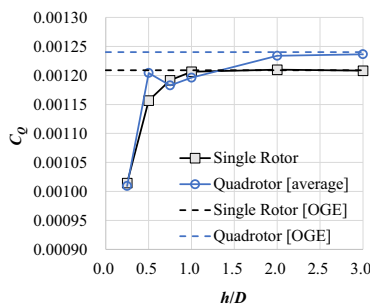


**Fig. 16.** Power consumption per rotor.

in **Fig. 14**. The rotor revolutions from the start are 30. It is observed that the rotors at  $h/D = 0.25, 0.5,$  and  $0.75$  are immersed within the rotor wakes.

The streamlines projected onto the vertical plane crossing two neighboring rotor centers are shown in **Fig. 15**. At  $h/D = 0.5$ , a strong flow recirculation was observed. Notably, the real streamlines in this type of flow field are unsteady and three-dimensional. However, the flow field for  $h/D = 0.5$  is different from that for  $h/D = 0.25$  and  $h/D = 0.75$ , where the downwash reflected by the ground is not sucked into the rotor. As shown in **Fig. 16**, where the torque coefficient for one of the quadrotors is shown together with the result for the single rotor, the torque coefficient for the quadrotor changes irregularly around the rotor height of  $0.5D$ . This corresponds to the flow recirculation observed in **Fig. 15** at the same rotor height. The ratios of  $C_Q$  in the ground effect (IGE) to  $C_Q$  OGE are shown in **Fig. 17**. The ground effect for the quadrotor starts to appear from a height of two rotor diameters, compared with a single rotor, for which the ground effect starts to appear from a height of one rotor diameter.

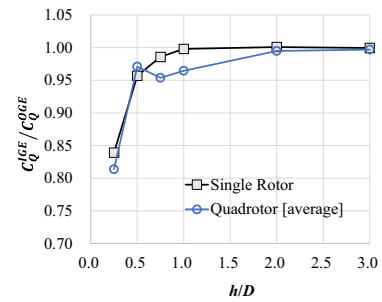


**Fig. 17.** Power consumption ratio due to the ground effect.

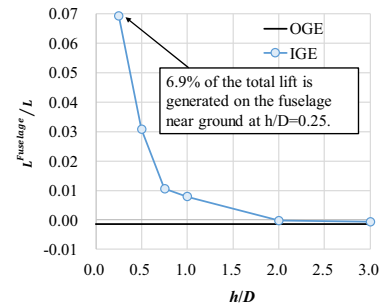


**Fig. 18.** Lift ratio acting on the fuselage.

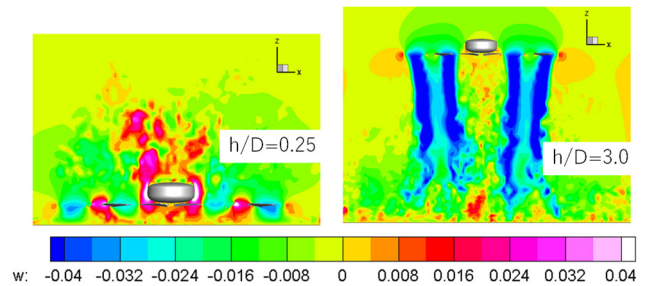


**Fig. 19.** Instantaneous velocity distribution on the central section of the quadrotor drone.

In the present simulations, the forces acting on the fuselage are not considered in the trim process. The lift generated by the fuselage,  $L^{Fuselage}$ , divided by the lift of the entire aircraft,  $L$ , is shown in **Fig. 18**. In the OGE condition,  $L^{Fuselage} / L$  was slightly negative, indicating a download on the fuselage. However, when the rotor height decreases, a positive lift is generated on the fuselage, indicating that there is an upwash around the central fuselage area, as shown in **Fig. 19**. The pressure coefficient ( $C_{pa}$ , pressure normalized based on sonic speed instead of uniform speed) distributions for  $h/D = 0.25$  and  $3.0$  on the central sections are shown in **Fig. 20**, where a high positive pressure can be observed on the bottom of the fuselage. The generation of lift on the fuselage corresponds to the power change caused by the ground effect. When the rotor height is  $0.25D$ , the lift ratio generated by the fuselage is approximately 6.9% of the lift generated by the rotors. A lift trim that includes the fuselage should be considered in future simulations.

For the case of the rotor at a height of  $0.5D$ , the aver-

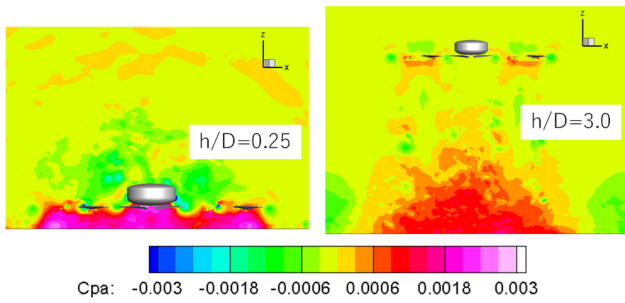


**Fig. 20.** Instantaneous pressure distribution on the central section of the quadrotor drone.

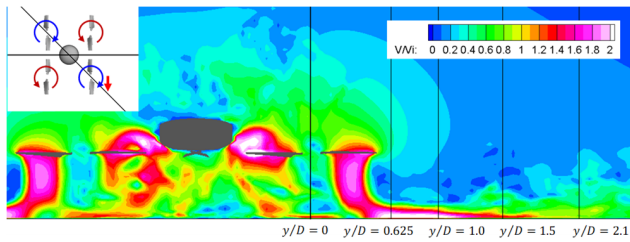


**Fig. 21.** Flow along the section crossing the diagonal rotor centers.

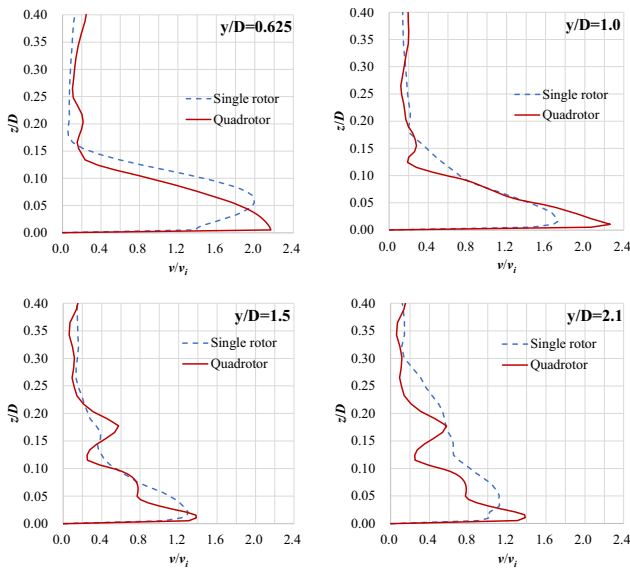


**Fig. 22.** Velocity profiles on the ground along the section crossing the diagonal rotor centers.

aged flow for two revolutions from 36 to 38 rotor revolutions is shown in **Fig. 21**, on the vertical plane crossing the diagonal rotor centers. The velocity profiles at  $y/D = 0.625, 1.0, 1.5,$  and  $2.1$  are shown in **Fig. 22**, indicating that the origin of  $y$  is located near the rotor center. The outwash along the ground is slightly higher than that induced by a single rotor, but the profiles appear similar.

In contrast, as shown in **Fig. 23**, a strong flow velocity also exists at high altitudes from the ground along the rotor gap center. Although the flow field shown here is averaged for two rotor revolutions, strong velocity fluctuations

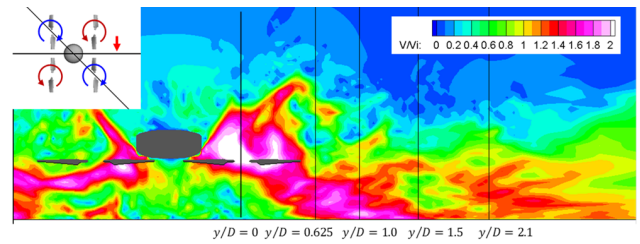


**Fig. 23.** Flow along the section of rotor gap center.

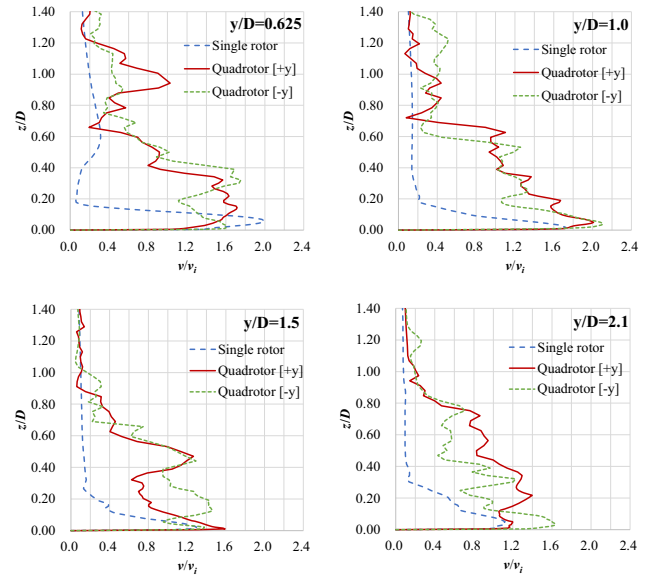


**Fig. 24.** Velocity profiles along the section of rotor gap center.

and asymmetry of the flow field can still be observed. As shown in **Fig. 24**, the maximum speed is approximately the same, but a strong wind up to a greater height from the ground is characteristically associated with the multiple rotors interacting in the ground effect. In addition, the velocity profiles obtained at the opposite side are shown for a comparison. There were some differences in the velocity profiles, but the heights at which a high velocity was reached were the same.

It is considered that the flow field around a multirotor drone near the ground is strongly unsteady in nature, and careful control is required. The quick response provided by the variable-pitch mechanism proposed in this study can contribute to the stable and robust control of multirotor drones. The change in the rotor gap and relative height may also influence the occurrence of the ground effect. This should be studied in the future for specific multirotor aircraft designs.

## 6. Conclusions

Numerical simulations of a single rotor and a quadrotor drone in the ground effect have been conducted.

- 1) For the single-rotor case, good agreement with existing empirical relations for the rotor in ground effect

has been confirmed. The predicted outwash on the ground was consistent with the existing experimental measurements.

- 2) Detailed flow field observations of the quadrotor hovering in the ground effect were obtained. It is observed that there is a flow recirculation for the quadrotor drone at an intermediate height of approximately 0.5 times the rotor diameter.
- 3) The required power of the quadrotor drone changes significantly with the rotor height from the ground. The local power increase is observed around a rotor height of  $0.5D$ . For an even lower rotor height, the rotor ground effect is consistent with that of the single-rotor case.
- 4) The velocity profile on the ground due to the outwash from the quadrotor drone changes significantly with the direction from the drone. Along the plane crossing the diagonal rotor centers, the velocity profile appears similar to that of a single rotor, although the maximum speed at the same station becomes slightly higher. However, along the plane between the rotor gap centers, the outwash exists up to a much higher altitude, where the maximum speed is almost the same as that of the single rotor.

#### Acknowledgements

This study was financially supported by JSPS KAKENHI JP19H02344, as part of research on the "Enhancement of safety of manned and unmanned multi-rotor aircraft and assessment of influences to surroundings."

#### References:

- [1] Y. Tanabe, S. Saito, N. Ooyama, and K. Hiraoka, "Study of a Downwash Caused by a Hovering Rotor in Ground Effect," Proc. of 34th European Rotorcraft Forum, Liverpool, UK, pp. 589-599, 2008.
- [2] I. C. Cheeseman and W. E. Bennett, "The effect of the ground on a helicopter rotor," ARC R&M, No.3021, pp. 1-10, 1955.
- [3] T. O'Bryan, "An Investigation of the effect of downwash from a VTOL aircraft and a helicopter in the ground environment," NASA Technical Note, D-977, 1961.
- [4] J. S. Hayden, "The effect of the ground on helicopter hover power required," Proc. of AHS 32nd Annual Forum, Washington, DC, pp. 1-11, 1976.
- [5] H. Usuda, N. Iboshi, and N. Itoga, "Ground effect of a hovering rotor over confined area," 45th Aircraft Symp., Kitakyushu, Japan, October 10-12, 2007 (in Japanese).
- [6] J. Schmaus, B. Berry, W. Gross, and P. Koliais, "Experimental Study of Rotor Performance in Deep Ground Effect with Application to a Human-Powered Helicopter," Proc. of American Helicopter Society 68th Annual Forum, Fort Worth, TX, pp. 1-12, 2012.
- [7] M. Sugiura, Y. Tanabe, H. Sugawara, N. Matayoshi, and H. Ishii, "Numerical Simulations and Measurements of the Helicopter Wake in Ground Effect," J. of Aircraft, Vol.54, No.1, pp. 209-219, 2017.
- [8] Y. Tanabe, T. Aoyama, M. Sugiura, H. Sugawara, S. Sunada, K. Yonezawa, and H. Tokutake, "Numerical Simulations of Aerodynamic Interactions Between Multiple Rotors," Proc. of 42nd European Rotorcraft Forum (ERF), Lille, France, 94, 2016.
- [9] M. Kohno, H. Otsuka, S. Kiribayashi, and K. Nagatani, "Investigation on Relationship between Rotors Axis Length and Ground Effect on a Small Quadrotor UAV Performance," Proc. of the Robotics and Mechatronics Conf. 2017 in Fukushima, 1P2-F02, 2017 (in Japanese).
- [10] M. Kohno, "Visualization of the Upstream Flow of Rotors and Analysis on Thrust of a Small Quadrotor UAV in Ground Effect," Proc. of 55th Aircraft Symp., Shimane, Japan, JSASS-2017-5022, 2017 (in Japanese).
- [11] K. Yonezawa, H. Matsumoto, K. Sugiyama, Y. Tanabe, H. Tokutake, and S. Sunada, "Aerodynamic Characteristics of a Quadrotor-Drone with Ducted Rotors," Proc. of 8th Asian/Australian Rotorcraft Forum, Ankara, Turkey, pp. 1-7, 2019.
- [12] Y. Tanabe, S. Saito, and H. Sugawara, "Construction and Validation of an Analysis Tool Chain for Rotorcraft Active Noise Reduction," Proc. of 38th European Rotorcraft Forum, Amsterdam, NL, pp. 235-247, 2012.
- [13] A. Hashimoto, K. Murakami, T. Aoyama, K. Ishiko, M. Hishida, M. Sakashita, and P. Lahur, "Toward the fastest unstructured CFD code 'FaSTAR'," Proc. of 50th AIAA Aerospace Sciences Meeting Including the New Horizons Forum and Aerospace Exposition, Nashville, Tennessee, AIAA-2012-1075, doi: 10.2514/6.2012-1075, 2012.
- [14] Y. Tanabe, S. Saito, O. Takayama, D. Sasaki, and K. Nakahashi, "A New Hybrid Method of Overlapping Structured Grids Combined with Unstructured Fuselage Grids for Rotorcraft Analysis," Proc. of 36th European Rotorcraft Forum, Paris, France, September 9-11, 2010.
- [15] Y. Tanabe, T. Aoyama, M. Sugiura, H. Sugawara, S. Sunada, K. Yonezawa, and H. Tokutake, "Multiple Rotors Hovering Near an Upper or a Side Wall," J. Robot. Mechatron., Vol.30, No.3, pp. 344-353, 2018.
- [16] E. Shima and K. Kitamura, "On New Simple Low-Dissipation Scheme of AUSM-Family for All Speeds," Proc. of 47th AIAA Aerospace Sciences Meeting, Orlando, FL, 2009-136, 2009.
- [17] Y. Tanabe and S. Saito, "Significance of All-Speed Scheme in Application to Rotorcraft CFD Simulations," Proc. of the 3rd Int. Basic Research Conf. on Rotorcraft Technology, Nanjing, China, 2009.
- [18] S. Yamamoto and H. Daiguji, "Higher-Order-Accurate Upwind Schemes for Solving the Compressible Euler and Navier-Stokes Equations," Computers and Fluids, Vol.22, No.2/3, pp. 259-270, 1993.
- [19] L. P. Zhang and Z. J. Wang, "A Block LU-SGS Implicit Dual Time-Stepping Algorithm for Hybrid Dynamic Meshes," Computers and Fluids, Vol.33, pp. 891-916, 2004.
- [20] A. Jameson and T. J. Baker, "Solution of the Euler equations for Complex Configuration," Proc. of 6th Computational Fluid Dynamics Conf. Danvers, Danvers, MA, USA, 83-1929, doi: 10.2514/6.1983-1929, 1983.
- [21] Y. Tanabe, H. Sugawara, K. Yonezawa, S. Sunada, and H. Tokutake, "Influence of Rotor Blade Twist on Ducted Rotor Performance," Proc. of 8th Asian/Australian Rotorcraft Forum, Ankara, Turkey, pp. 1-6, 2019.

#### Supporting Online Materials:

- [a] Uber Elevate eCRM-004. <https://evtol.news/uber-elevate-ecrm-004/> [Accessed October 9, 2020]
- [b] <https://evtol.news> [Accessed October 9, 2020]



#### Name:

Yasutada Tanabe

#### Affiliation:

Senior Researcher, Japan Aerospace Exploration Agency (JAXA)

#### Address:

6-13-1 Osawa, Mitaka, Tokyo 181-0015, Japan

#### Brief Biographical History:

1991- Kawada Industries, Inc.

2006- Japan Aerospace Exploration Agency (JAXA)

#### Main Works:

- "Multiple Rotors Hovering Near an Upper or a Side Wall," J. Robot. Mechatron., Vol.30, No.3, pp. 344-353, 2018.

#### Membership in Academic Societies:

- The Japan Society of Aeronautical and Space Sciences (JSASS)
- The Vertical Flight Society (VFS)
- Japan Helicopter Society (JHS)



**Name:**  
Hideaki Sugawara

**Affiliation:**  
Researcher, Japan Aerospace Exploration Agency (JAXA)

**Address:**  
6-13-1 Osawa, Mitaka, Tokyo 181-0015, Japan

**Brief Biographical History:**  
2007- Ryoyu Systems Co., Ltd.  
2020- Japan Aerospace Exploration Agency (JAXA)

**Main Works:**  
• “Numerical Investigation of Rotor/Wing Aerodynamic Interactions at High Advance Ratios,” J. of Aircraft, Vol.56, No.6, pp. 2285-2298, 2019.

**Membership in Academic Societies:**  
• The Japan Society of Aeronautical and Space Sciences (JSASS)  
• The Vertical Flight Society (VFS)



**Name:**  
Shigeru Sunada

**Affiliation:**  
Professor, Nagoya University

**Address:**  
Furo-cho, Chikusa-ku, Nagoya, Aichi 464-8603, Japan

**Brief Biographical History:**  
1992- Researcher, Kawachi Millibioflight Project, ERATO, JST  
1997- Senior Researcher, National Institute of Advanced Industrial Science and Technology (AIST)  
2001- Assistant Professor, Osaka Prefecture University  
2017- Professor, Nagoya University

**Main Works:**  
• Y. Tanabe, K. Yonezawa, H. Tokutake, S. Suzuki, K. Yamaguchi, and S. Sunada, “A study on enhancing the agility and safety and on increasing the flight duration of a multiple rotor drone,” S. Tadokoro (Ed.), “Disaster Robotics,” Springer, pp. 111-122, 2019.

**Membership in Academic Societies:**  
• The Japan Society of Aeronautical and Space Sciences (JSASS)  
• The American Institute of Aeronautics and Astronautics (AIAA)  
• The Robotics Society of Japan (RSJ)



**Name:**  
Koichi Yonezawa

**Affiliation:**  
Civil Engineering Laboratory, Central Research Institute of Electric Power Industry

**Address:**  
1646 Abiko, Abiko-shi, Chiba 270-1194, Japan

**Brief Biographical History:**  
2002- Research Associate, Osaka University  
2007- Assistant Professor, Osaka University  
2017- Central Research Institute of Electric Power Industry

**Main Works:**  
• “Propeller Design and Loss Mechanisms in Low-Reynolds-Number Flows,” J. of Propulsion and Power, 2016.

**Membership in Academic Societies:**  
• The Japan Society of Mechanical Engineers (JSME)  
• Turbomachinery Society of Japan (TSJ)



**Name:**  
Hiroshi Tokutake

**Affiliation:**  
Professor, Kanazawa University

**Address:**  
Kakuma-machi, Kanazawa, Ishikawa 920-1192, Japan

**Brief Biographical History:**  
1997- Research Associate, Osaka Prefecture University  
2010- Associate Professor, Kanazawa University  
2018- Professor, Kanazawa University

**Main Works:**  
• “Exploration of Wind Structure on Mars using an Airplane and Flight Feasibility Study,” Trans. of the Japan Society for Aeronautical and Space Sciences, Vol.60, pp. 212-220, 2017.

**Membership in Academic Societies:**  
• The Japan Society of Aeronautical and Space Sciences (JSASS)  
• The American Institute of Aeronautics and Astronautics (AIAA)  
• The Society of Instrument and Control Engineers (SICE)  
• Society of Automotive Engineers of Japan (JSAE)